Yin, F., Lühr, H., Park, J., Rauberg, J., Michaelis, I. (2015): Noise features of the CHAMP vector magnetometer in the 1–25Hz frequency range. - *Sensors and Actuators A - Physical*, *222*, p. 272-283.

DOI: http://doi.org/10.1016/j.sna.2014.12.024

Noise Features of the CHAMP Vector Magnetometer in the 1-25 Hz Frequency Range

Fan Yin[1,3] Hermann Lühr[2, 1] Jaeheung Park[2] Jan Rauberg[2] Ingo Michaelis[2]

[1] Department of Space Physics, College of Electronic Information, Wuhan University, 430072 Wuhan, People's Republic of China

[2] Helmholtz-Centre Potsdam, GFZ-German Research Centre for Geosciences, Telegrafenberg, 14473 Potsdam, Germany

E-mail:yinfan@whu.edu.cn

Abstract. CHAMP (CHAllenging Minisatellite Payload), a German small satellite mission to study the Earth's gravity field, magnetic field and upper atmosphere, ended in space on 19 September 2010. Thanks to the good quality of the satellite and to several altitude maneuvers, the satellite provided continuous and reliable observations including house-keeping data at different processing levels for more than 10 years. Among them the high-resolution vector magnetic field data, provided by the FGM (FluxGate vector Magnetometer) at 50Hz sample rate, are one of the most important data products. The 50Hz data allows us to investigate all signals from DC to 25Hz. Here we report on noise features found in the frequency range above 1Hz. There are predominantly three types of disturbances found regularly in the vector magnetic field data. One is at ~2.1Hz and harmonic signals, an other is an 8Hz single frequency signal. The features of these two signals are characterized and analyzed, which helps

us to trace the signals to the source of disturbance. The 2.1Hz harmonic signals mainly depend on the incident angle of sunlight, which points at the star tracker instrument ASC (Advanced Stellar Compass), as the signal depends on the level of blinding. The 8Hz sinusoidal signal is continuously present and its amplitude is controlled by the temperature inside of the satellite. For higher temperatures the signal gets smaller, and it practically disappears above 20°C. Only the FGM x-axis is affected by the 8Hz signal. The third artificial signal affects the FGM y-axis. A frequency sweep from the Nyquist frequency down to zero and up again occurs when the readings of the FGM y-axis go through zero. This is probably related to a ringing of the analog-to-digital converter at the sign change. The amplitudes of all these noise features are generally below 50 pT.

Keywords: CHAMP satellite, Flux-Gate vector Magnetometer, Magnetometer noise, Time-frequency analysis

1. Introduction

The CHAMP satellite was launched on 15 July 2000 into an 87.3 degrees inclined circular orbit with 454 km altitude, and reentered the atmosphere at about 250 km altitude on 19 September 2010 (Lühr et al. 2013). One of the prime objectives was the measurement of the Earth's magnetic field. For that purpose CHAMP carried a magnetometer instrument package consisting of an Overhauser scalar magnetometer (OVM) manufactured by Laboratoire d'Electronique de Technologie et d'Instrumentation, LETI, France and two Fluxgate vector magnetometers (FGM) and a pair of star sensors (ASC), both manufactured by the Technical University of Denmark, DTU, (Reigber et al. 2002). These two FGMs (one served as redundant unit) were rigidly mounted on an optical bench on the 4-meter boom together with the two star sensors providing precise attitude information. For more information on payload accommodation see Figure 1 and Lühr et al. (2013). CHAMP flew with the boom in forward direction,

[3] To whom any correspondence should be addressed.

During the mission CHAMP sampled besides the dominant geomagnetic core field and the moderate lithospheric magnetic field also magnetic signals from ionospheric and magnetospheric currents due to its high precision and resolution. The 50 Hz sample rate of the FGM allows the investigation of phenomena in the Extreme Low-Frequency (ELF) range up to the Nyquist frequency of 25 Hz. Examples of performed studies in that frequency range using CHAMP data are the survey of Pc1 pulsations (Park et al., 2013), characteristics of kilometer-scale field-aligned currents (Rother et al., 2007), or the fine-structure of equatorial plasma irregularities (Lühr et al., 2014a, b).

A phenomenon in the ELF range worth mentioning is the Schumann resonances (SRes), which forms in the Earth-ionosphere waveguide (Schumann 1952). Ni and Zhao (2005) claimed that they had detected magnetic and electric signatures of SRes in the upper ionosphere (~640 km altitude) based on the power spectrum analysis of Aureol-3 satellite electromagnetic wave measurements. Simões et al. (2011) reported that the SRes (at 7.8, 14.3, 20.8, 27.3, and 33.8 Hz signals) are routinely observed in the electric field data of the C/NOFS satellite during nighttime conditions within the altitude range of 400-850 km. Surkov et al. (2013) have theoretically confirmed the feasibility of SRes observation by low orbiting satellites in the topside ionosphere. Several of the SRes harmonics fall into the CHAMP measurement range.

However, some signals discovered in the CHMP magnetometer data might be related to artificial disturbances from the satellite. For example the 50mHz signals in CHAMP magnetic field data can be traced back to an imperfect correction of the magneto-torquer signals (Yin et al. 2013).

In this article we will investigate the disturbance signals in CHAMP 50Hz magnetic field data and present their characteristics. For any scientific study in the ELF range it is essential to know the artificial signals and take them properly into account. In the sections to follow we first introduce the data processing approach and subsequently present and interpret the three main disturbance signals observed in the CHAMP data within the ELF range. The Conclusion section provides actual numbers for the disturbance levels.

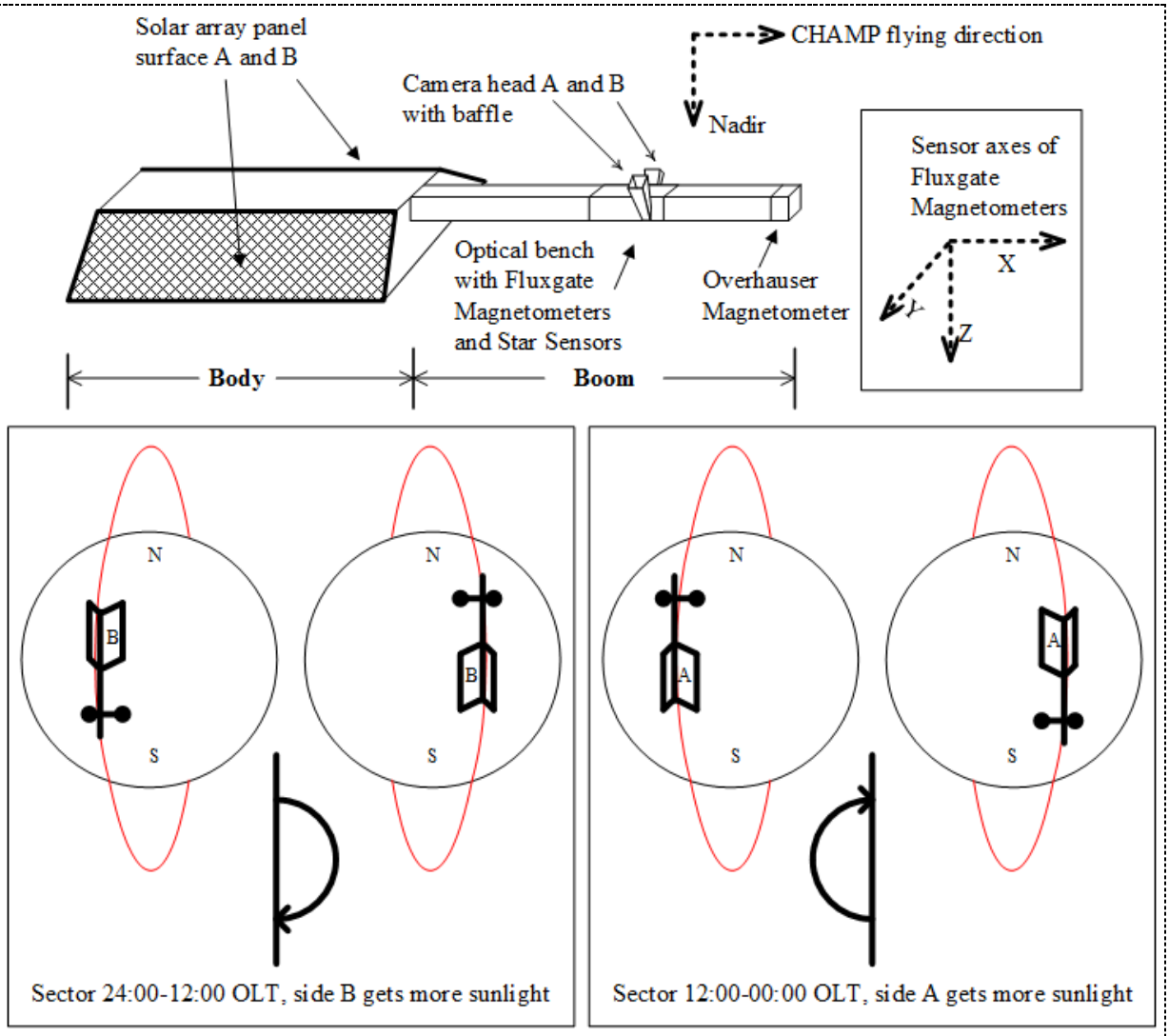

Figure 1. Schematic illustration of the CHAMP satellite (top) and a schematic relationship between CHAMP attitude in orbit and sunlight (bottom).

2. Processing approach and spectral overview

For the study presented here we have used the CHAMP 50Hz data of the FGM measurements. The FGM sensor is oriented such that the x-axis is aligned with the boom and points in flight direction. The y-axis points sideways lying in the horizontal plane. Thus the x and y axes measure approximately the northward and eastward (southward and westward) components of the magnetic field during upleg (downleg) orbital arcs. The z-axis is always sampling the downward component (see Fig. 1). In

77 nominal operation the ambient magnetic field was measured by the FGM at a rate of 50 Hz with a
78 resolution of 10 pT over a range from -65000 nT to 65000 nT.
79 For this study the FGM data have been transformed into the Mean-Field-Aligned (MFA) coordinate
80 system. This frame allows for a better separation between natural and artificial signals. Most natural
81 signals are confined to the two transverse magnetic components. In the MFA frame the z component,
82 "parallel," is aligned with the mean field, the y component, "zonal," is perpendicular to the mean field
83 and is pointing to the east, and the x component, "meridional," completes the triad and points outward.
84 A more detailed description of that frame can be found in Park et al. (2013). In this frame x and y
85 signals are generally small and z comprises the total field strength. In order to interpret disturbance
86 signals we have considered also some instrument house-keeping (HK) data such as temperature and
87 instrument operational modes for comparison.
88 Our basic method is spectral analysis. There are many different techniques for harmonic analysis, such
89 as discrete Fourier transform (DFT), periodogram or wavelets. However, the issue here is not the
90 method per se. In fact no marked difference can be observed between using different methods of
91 spectrum analysis when searching for artificial signals. From the perspective of consistency the spectra
92 in this work are power spectral density (PSD) using Welch's method for a comprehensive
93 consideration.
94 For our analysis we first divide the FGM data into the ascending orbital arc (from south pole to north
95 pole) and descending arc (from north pole to south pole). Here we focused on the signals above 1Hz,
96 therefore the large contributions, e.g. from the Earth's core field have been subtracted by applying a
97 smoothing cubic spline fitting with appropriate parameters. This kind of tactics is more efficient and
98 convenient for our purpose than the usually way of removing the mean field by a geomagnetic field
99 model. For each arc we calculate the spectrum to identify frequencies of enhanced signals. Figure 2,
100 left frames, give an example of the PSD versus frequency for MJD 3215 (Modified Julian Day is
101 counting from 01-01-2000). Some spectral peaks can clearly be identified: one is at 2.1 Hz (more
102 precisely 2.1025 Hz) with its harmonic at 4.2 Hz, 6.3 Hz, 8.4 Hz etc.; another feature is an 8 Hz

single-frequency signal. The former peaks appear only on descending arcs, but the latter appears on all the arcs. The Orbital Local Time (OLT: local time at ascending node, it repeats after about 261 days for CHAMP) on MJD 3215 was about 01:34. The descending arcs were on the dayside, which indicated that the 2.1 Hz harmonic signals might be related to sunlight. In Figure 2, right frame, the 8 Hz signals shows weak sidebands at 8 Hz $\pm$~0.1 Hz. Such sidebands indicate a modulation of the 8 Hz signal at a period of about10 seconds. Presently we have no conclusive explanation for it. Larger sidebands appear at 8 Hz $\pm$1 Hz. This latter modulation is probably related to the synchronization of the satellite operation to the GPS Pulse Per Second (PPS).

Although the spectrum derived from a long time sequence gives us a good insight into the frequency resolution, it obscures the temporal evolution. In order to determine when and where these signals appear a time-frequency analysis is applied. The input FGM data are divided into many shorter segments with overlaps between neighboring segments. For each segment we can calculate the short-term, time-localized spectrum. Consequently, a dynamic spectral density distribution with time and frequency resolution can be derived. The resolution in time and frequency depends on the separation between segments and the segment length, respectively. After testing several options we choose 4 minutes for the segment length and 15 seconds for the separation between spectra as a compromise with regard to resolution and efficiency. This combination provides spectrograms with about 0.004 Hz frequency resolution and a spatial resolution of about 1 degree in latitude. Figure 3 shows as an example the frequency-time (F-T) spectrogram of B_z (MFA) for one day, MJD 3208. Both the 8 Hz signal and 2.1 Hz harmonic signals can clearly be distinguished from the background noise. Notice that on this day the 2.1 Hz signals appear not only on dayside but also on the nightside.

These two kinds of signal reported here are typical for most of the CHAMP orbits. Investigation of these effects requires a large number of data over years. For getting a better overview of the occurrence of disturbances, times are flagged as events when the PSD magnitude is above a certain threshold. After some tests we selected for the 2.1 Hz harmonic signals a PSD magnitude threshold of 0.0006 nT^2/Hz, and for the 8 Hz signals the PSD magnitude of 0.0003 nT^2/Hz. A larger threshold leads

to more omissions and a smaller one leads to more misinterpretation of noise, which both obscures the pattern recognition. The threshold for the 2.1 Hz signal is derived from the average PSD magnitude of the first three harmonics. In case of the 8 Hz signal the spectral peak around 8 Hz is directly used.

For each detected event we can get the time information (date and local time) and position (latitude and longitude). Thus, a quad of parameters (time, latitude, longitude, magnitude) is accompanying the events. In total we have derived about 400,000 events from the years 2007 and 2008 for the 2.1 Hz harmonics in the MFA z component, while there are about 2,800,000 events from 2008 for the 8Hz signal when considering all three field components. In the next sections we will present the characteristics of the disturbances in more detail.

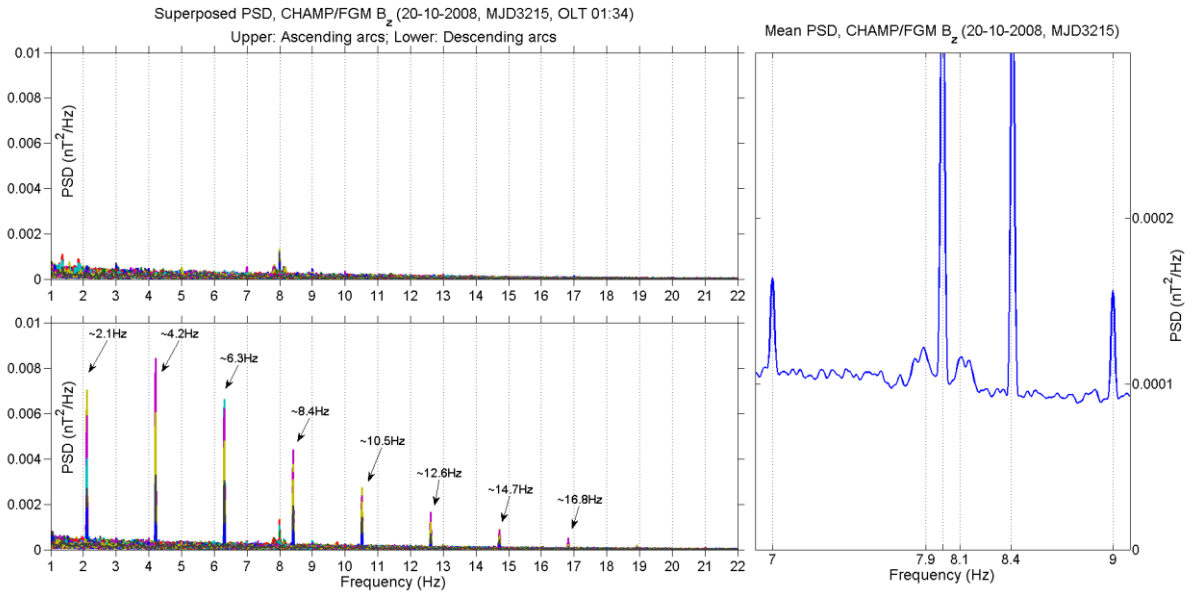

Figure 2. Noise spectrum of one day: superposed PSD of B_z (in MFA) for MJD 3215. (upper left) ascending arcs at 01:34 OLT, (lower left) descending arcs at 13:34 OLT; (right frame) zoomed spectrum with sidebands of the 8 Hz signal.

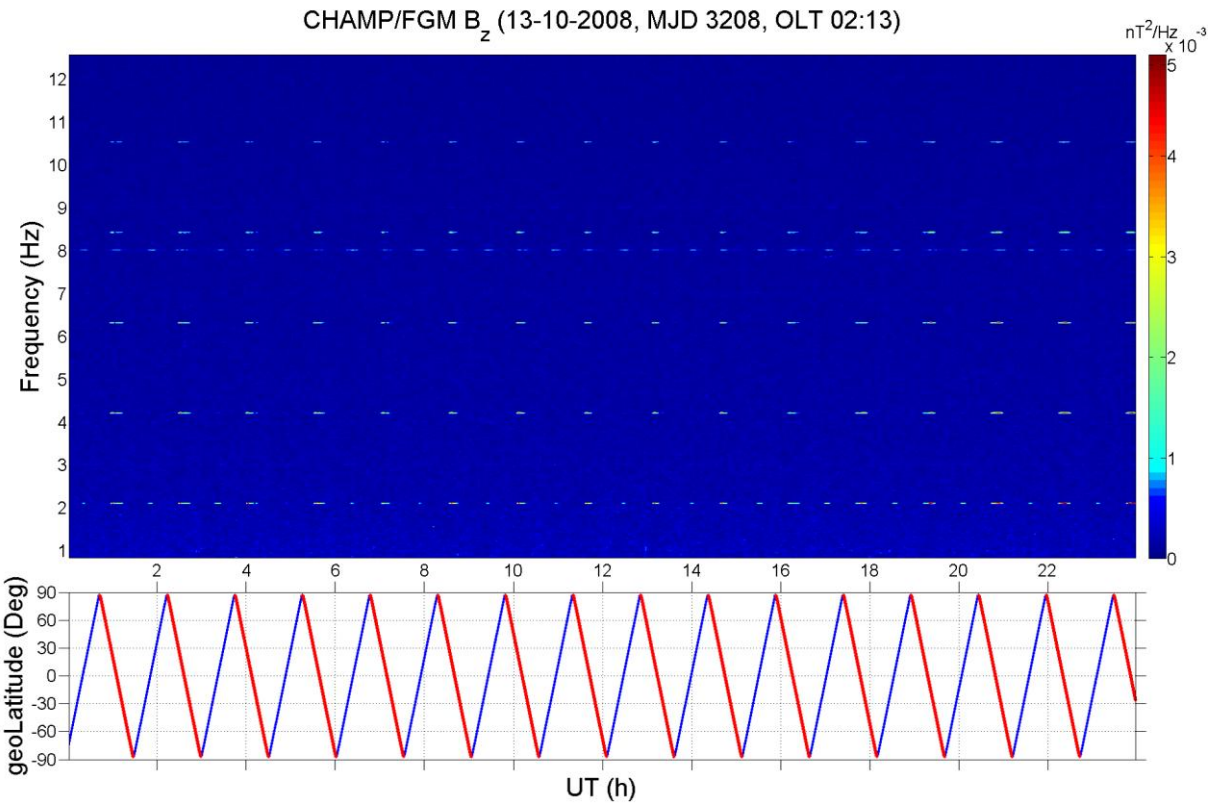

Figure 3. Dynamic noise spectrum of B_z (in MFA) for MJD 3208. (lower frame) latitudinal of CHAMP position (blue: ascending arcs; red: descending arcs). Local time of the ascending node is 02:13 OLT.

3. Characteristics of disturbance signals

Based on the large number of detected events accompanied by time, latitude, longitude, and magnitude we can efficiently obtain the typical characteristics of the signals, which help us to trace the possible sources of the signals. In the following subsections observed details of the disturbance distribution are presented and interpretations are provided.

3.1 Features of the 2.1 Hz harmonics signal

148 The 2.1 Hz signals are present in all three field components and the spectral amplitudes are consistent
149 with each other in time frame. For that reason we present here only the observations of 2.1 Hz
150 disturbance in the MFA z component due to its low contamination by natural signals. The primary key
151 parameter for sorting the data is time, which assures uniqueness. With respect to time various
152 parameters can be used for presentation. The word "distribution" hereafter, if not specified differently,
153 means the event distributed in different sub-frames (e.g. time-latitude, time-magnitude, longitude-
154 latitude).

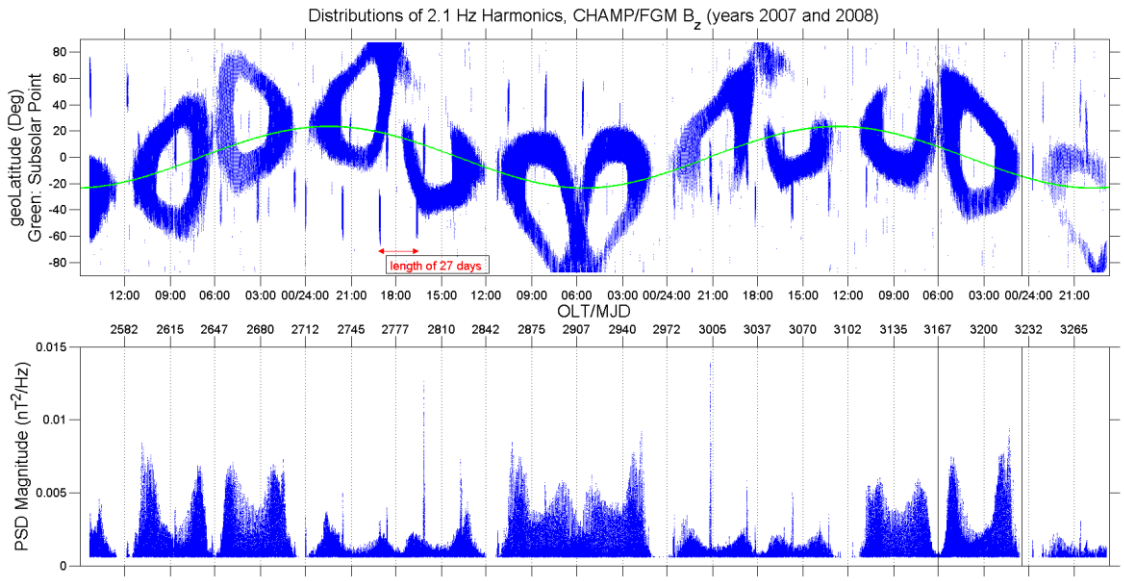

Figure 4. Event distributions of 2.1 Hz harmonic signals. (top) event occurrence in time-latitude frame; (bottom) magnitude distribution in time-magnitude frame.

155

156 The primary part of the 2.1Hz harmonics appears on the dayside. Figure 4 shows the distributions of
157 2.1Hz harmonics for the years 2007 and 2008 in different frames. From them the distributions in
158 latitude and related amplitudes can easily be recognized. The main structures (fully-closed and half-
159 open rings) in time-latitude frame follow the latitude of sub-solar points. In addition, OLT strongly
160 controls the signals, but also the season plays a role. The pattern in the time-magnitude frame indicates
161 the variation of the maximum magnitude over time. The vertical center lines through the rings are

located at about 03:00, 09:00, 15:00, 21:00 OLT accompanied by weaker magnitude than at the brim lines. An M-type shape of the time-magnitude variation corresponds with the ring structure in the time-latitude frame. In a 3-D representation it looks like a sequence of volcanic crater. The diameter of a ring spans almost 6 hours in OLT or 65 days. Around 00:00, and 12:00 OLT the 2.1 Hz signal is practically absent, and around 06:00 and 18:00 OLT it is strongly suppressed with some dependence on season.

From the lower frame of Figure 4 it is obvious that the PSD magnitude varies at a 12 h OLT period. During the sector 00:00 to 12:00 OLT, when the sun shines on the A-side of the satellite, the disturbance amplitude is significant larger than during the sector 12:00 to 24:00 OLT with the sun on the B-side. For the definition of the satellite sides see Figure 1. In general, sunlight plays a key role for the signals. Furthermore, tens of vertical stripes can be seen in the time-latitude frame of Figure 4 (some are obscured by the ring structures). Some of them are accompanied by extra large magnitudes compared to their neighbors (see Figure 4, lower frame). The vertical stripes repeat at a period of about 27 days. If we trace them back to the T-F spectrogram, it is found that they are single frequency 2.1 Hz signals (the higher harmonics are strongly depressed). As showed in Figure 3 these extra signals appear on the nightside. Evidently, moonlight should be responsible for that. This is supported by the period of about 27 days. Park et al. (2012) showed that the Doppler-shifted lunar period in CHAMP data is 26.52 days. Furthermore, Figure 5 discloses that at the time and position represented by the vertical stripes (mainly on nightside) the elevation of the moon is commonly around 45 degree.

There is also some fine structure, which can be found in the distribution pattern. Let us have a closer look at a single ring in time-latitude frame. Figure 6 upper and middle panels show a zoomed period, MJD 3167 to 3227, which is marked by two solid vertical lines in Figure 4. In the same way, the lower frame of Figure 6 represents a further zoomed period, MJD 3180 to 3190. There appears a diurnal variation of the event distribution forming the ring shape in time-latitude frame and a synchronous modulation of the M-shape in time-magnitude frame. This diurnal variation reflects some kind of longitude dependence. From Figure 7 we can see that the magnitude of the disturbance has a clear

188 longitude dependence that follows magnetic latitudes, particularly in the southern hemisphere. We do
189 not think that the strength of disturbance depends on longitude, but our result reflects rather the angle
190 between the disturbance vector and the ambient magnetic field direction, since we show only the MFA
191 Bz component. In particularly, in the southern hemisphere in the region of the South Atlantic Anomaly
192 the magnetic field is deviating a lot from the dipole orientation, in contrast to the northern hemisphere.
193 After having shown the details of the observed artificial 2.1 Hz signals we want to make suggestions
194 on the disturbance source. A very convincing fingerprint is the frequency of spectral peaks. The star
195 sensor unit is the only one that is not synchronized with the GPS Pulse Per Second. It runs a little
196 faster at a frequency of 1.051 Hz. This is just half the frequency of the fundamental disturbance signal.
197 It provides strong evidence for the ASC to be the source of the artificial signals. The many harmonics
198 spectral lines indicate that the original signal must be a narrow spike, similar to a delta-function. This
199 spike must appear about twice per operation cycle, due to the 2-Hz separation between the spectral
200 peaks. When looking into the 50 Hz time series, one can identify with some imagination spikes at 0.5 s
201 separations with amplitudes of about 0.1 nT.
202 The ASC comprises two camera heads, one on the A-side and the other on the B-side of the satellite.
203 Depending on the attitude with respect to the sun one of the cameras is blinded. Interestingly, the
204 disturbances disappear when a complete blinding occurs (see open areas within the rings in Fig. 4).
205 The magnetic spikes seem to appear at the transition into the blinding. During the orbits around
206 12:00/24:00 OLT none of the heads is blinded. Consequently, no disturbance signals are observed.
207 From Figure 4 it is evident that the PSD magnitude is larger during 03:00-09:00 OLT that means the
208 star camera on the A-side of the satellite produces stronger disturbances. Also the moon causes the
209 generation of disturbance spikes. The 2.1 Hz signals on the nightside appear, as expected, around the
210 epoch of moon transitions through the camera. The absence of higher harmonics suggests that the
211 disturbance signal is more sinusoidal in the case of moon sighting. In particular during equinoxes both
212 cameras can be blinded, one by the sun, the other by the moon. That may be the reason why we
213 observe very large PSD magnitudes during those particular days (see Fig. 4).

From all the presented arguments we conclude that the ASC is the source of the 2.1 Hz harmonics signal during certain operational conditions.

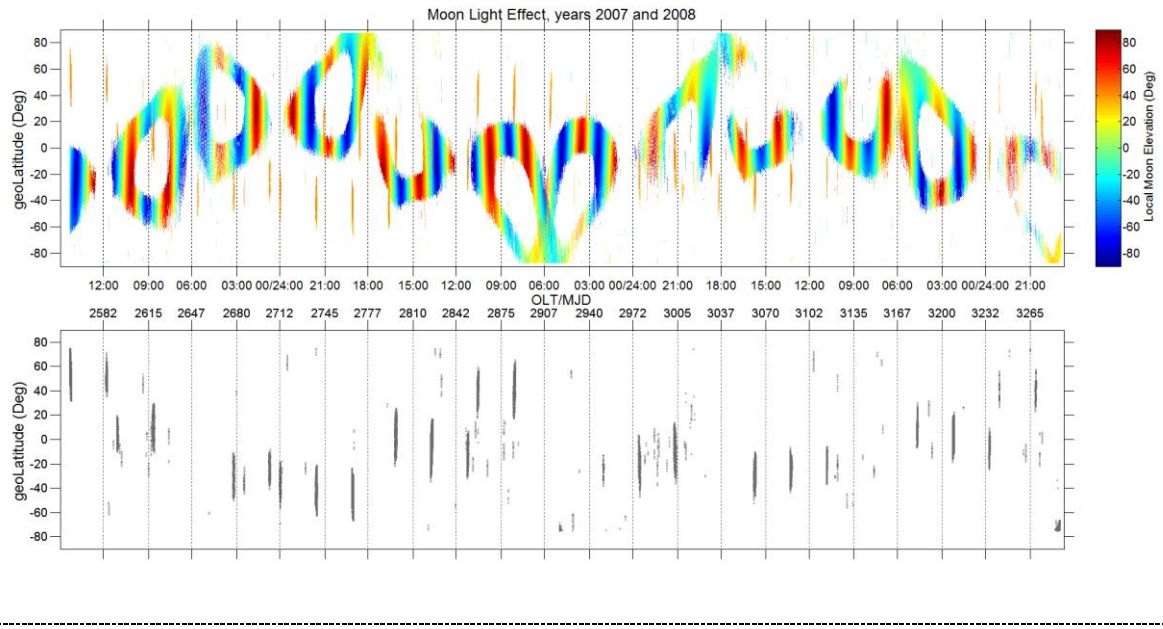

Figure 5. Upper: Event distributions of 2.1 Hz harmonic signals with respect to moon elevation. (top) color coded event occurrence in time-latitude frame; (bottom) event distribution on the nightside.

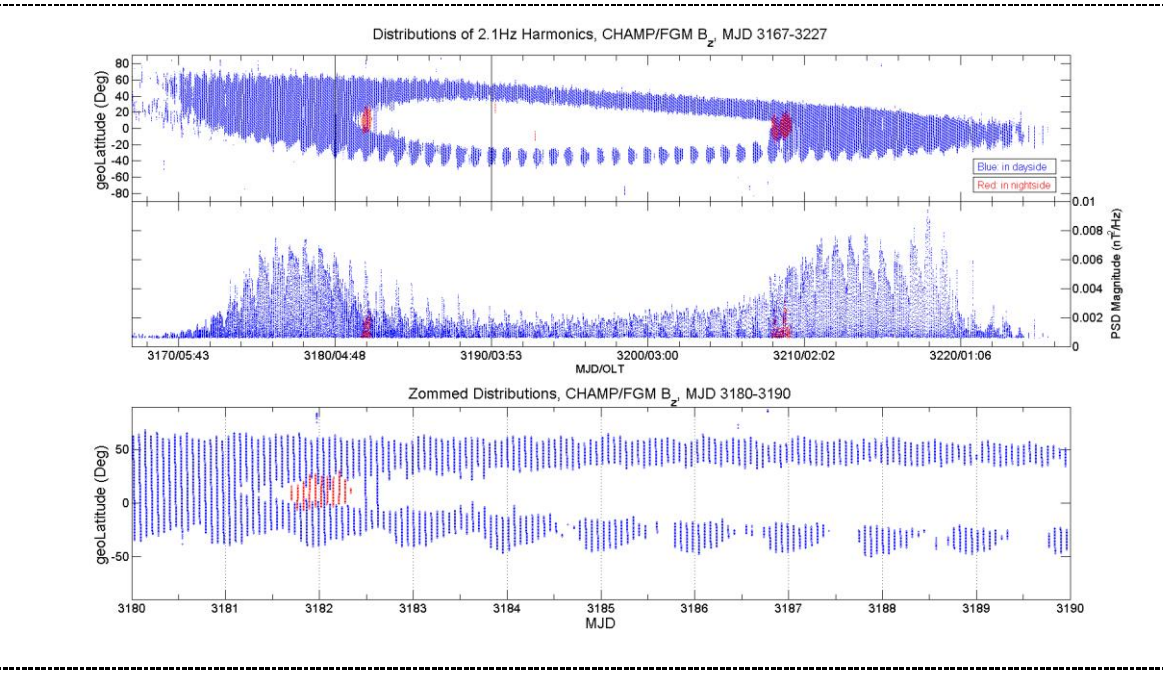

Figure 6. Event distributions of 2.1 Hz harmonics at expanded scale. (top panel) event occurrence in time-latitude frame over 60 days; (middle panel) PSD magnitude distribution; (bottom frame) details of event occurrences over 10 days. The red stripes mark events caused by moonlight.

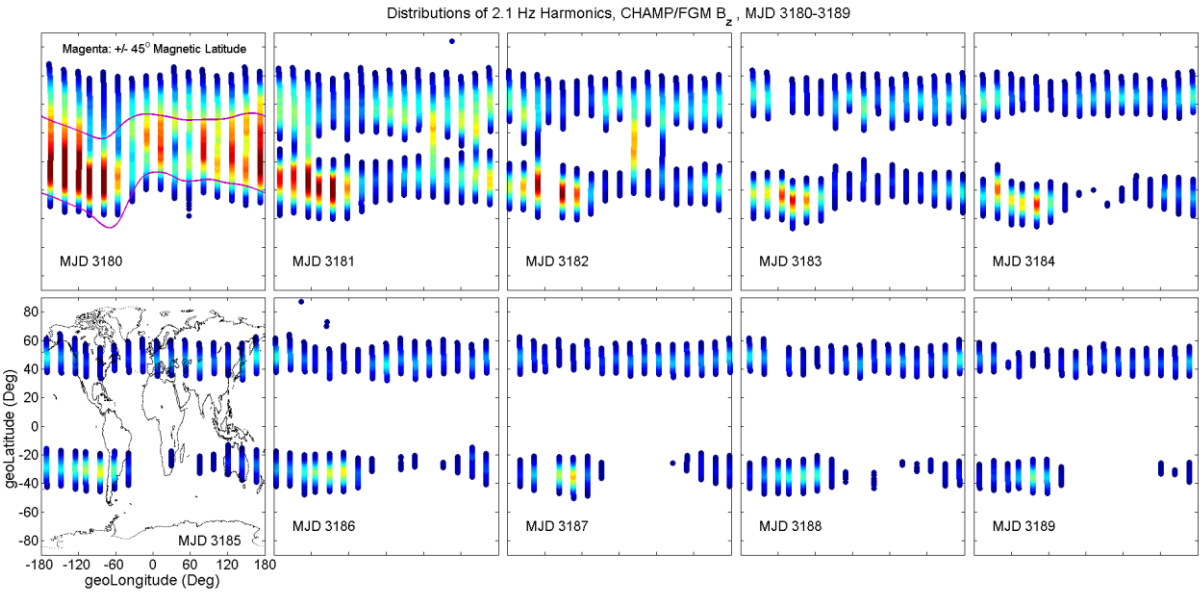

Figure 7. Day-to-days event distributions of the 2.1 Hz harmonics in a longitude-latitude frame spanning MJD3180-3189. Warm colors reflect high PSD magnitudes. Data from the nightside are excluded.

3.2 Features of the 8 Hz signal

The 8 Hz single frequency signal is different from the 2.1 Hz harmonics. It appears on every ascending/descending arc and lasts longer time. Sun light plays no role for it. In contrast, temperature is a key parameter for the appearance. From Figure 8 we can clearly recognize this feature of the 8 Hz signal. At relatively high temperatures, above 19°C, the signal is strongly suppressed in strength at all latitudes. The temperature inside of the satellite depends on the incidence angle of sunlight on the satellite body. Some cases of the attitude maneuvers confirm this relation and the role of temperature. For example, during the attitude maneuver on MJD 3091-3092 (from 2008-Jun-18 16:00 UT to 2008-

227 Jun-19 07:00 UT) when the temperature dropped by several degrees the 8 Hz events appeared with
228 much stronger amplitude than usually. All the spikes in the time-magnitude chart (Fig. 8) are well
229 correlated with the decreases of the Analog-to-Digital Converter (ADC) temperature.
230 So far we have considered only the 8 Hz signal in the MFA B_z component. The question is how much
231 the other components are affected. Figure 9 shows the event distribution in all three MFA components.
232 For the distribution map of the 8 Hz signals we have binned the events into a 1^o longitude × 1^o latitude
233 grid. A very clear pattern emerges reflecting the geomagnetic field geometry. The z component detects
234 the 8 Hz signal at low magnetic latitudes. At higher latitudes the x component takes over. In the y
235 component we only find events at higher latitudes and in regions with large declination, partly
236 approaching 90°, e.g. in the southern hemisphere around 80°E longitude. All these features are
237 consistent with the conclusion that the 8 Hz signal is a phenomena of the FGM x-axis sensor and it is
238 present all the time. In order to confirm this inference we have analyzed the noise spectrum separately
239 for the three FGM sensor axes for the day MJD 3180. The result clearly confirms that only the x-axis
240 is affected by 8 Hz. An interesting observation is that the 8 Hz signal of the FGM x-axis is temperature
241 dependent. At lower temperature the amplitude gets larger, and above 19°C the ringing practically
242 disappears. This feature may help to identify the root cause of the phenomena.
243

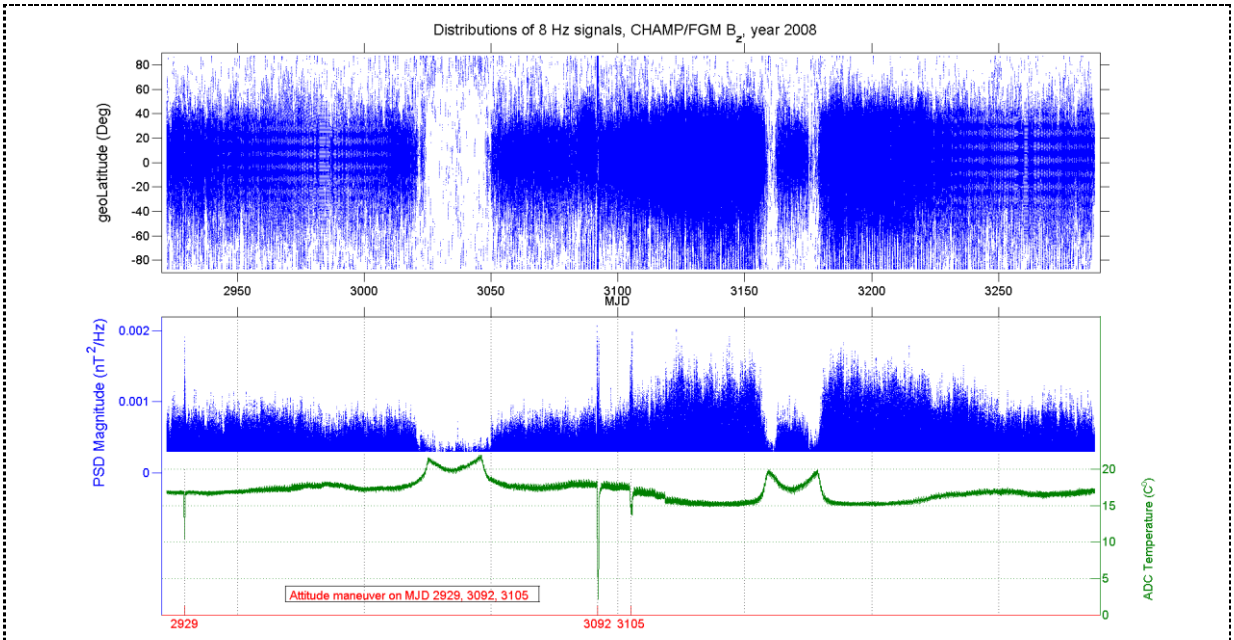

Figure 8. Temperature dependence of 8 the Hz signal. (top) event occurrence in time-latitude frame; (middle panel) magnitude distribution in time-magnitude frame; (bottom frame) temperature variation of the magnetometer ADC.

244

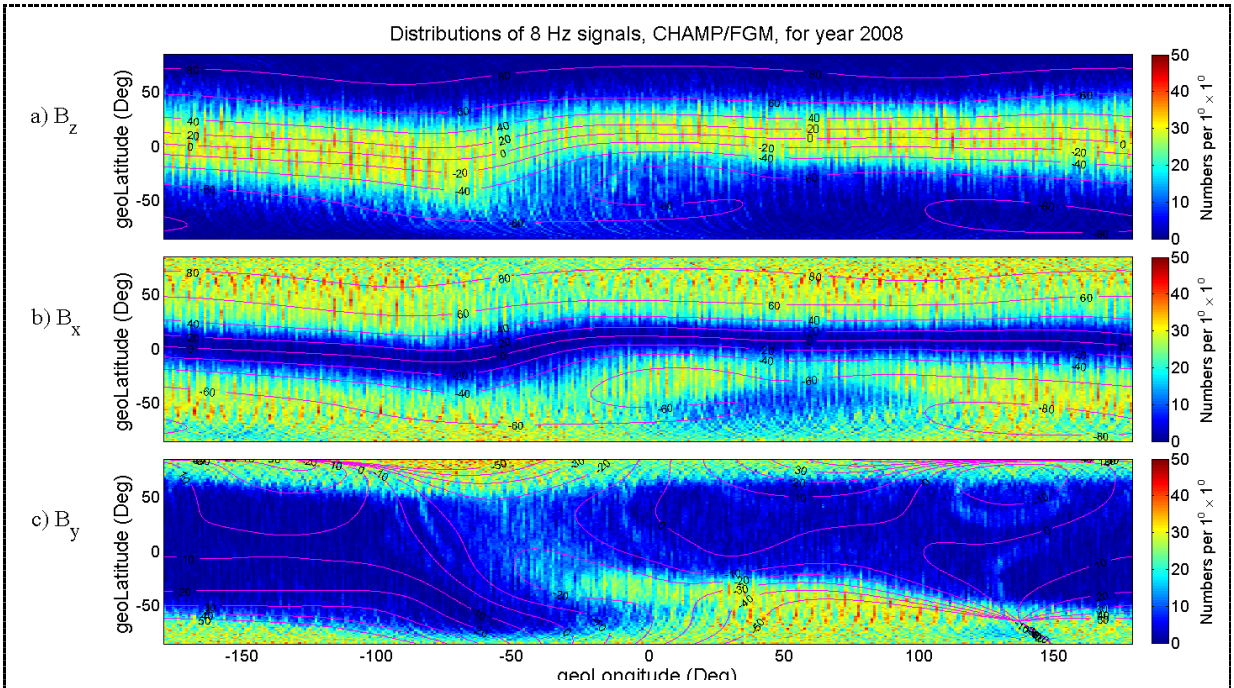

Figure 9. Global event occurrence distributions of the 8 Hz signal in the three MFA components: B_z

top, B_x middle, B_y bottom, for the year 2008. The lines in the two upper frames represent magnetic inclination, in the bottom frame it is magnetic declination.

3.3 Artificial signals of the FGM y-axis

When looking at the bottom frame of Figure 9 one sees some light blue patterns in the By signal at low and middle latitudes. These signals cannot be related to the 8 Hz ringing of the FGM x-axis. We have traced them back in the time series data. Figure 10 shows an example of such an event. There appears a clear ELF burst in the zonal, By component around 40° MLat (magnetic latitude), but nothing is seen in the meridional, Bx component. Corresponding to this burst the dynamic spectra below show a W-shaped feature. In the beginning we had no viable explanation for this peculiar feature and did not know whether it is a natural or artificial signal.

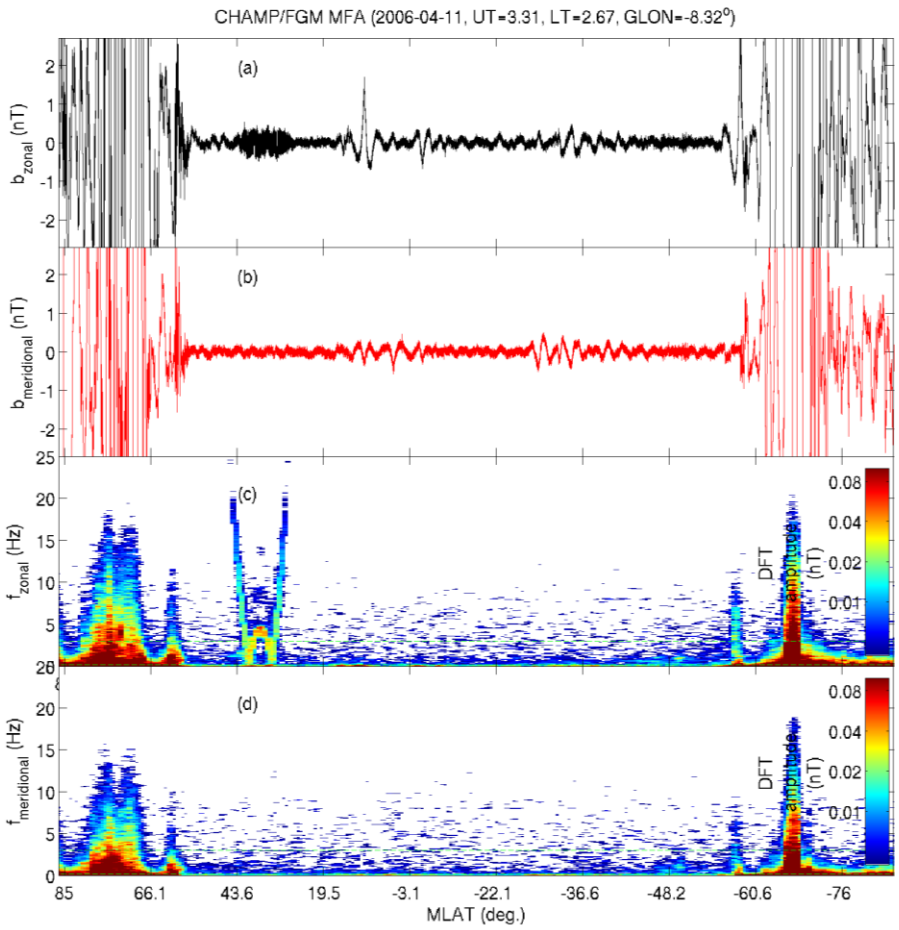

Figure 10. Example of a W-shaped event. The two panels (a) and (b) show time series of the MFA B_y and B_x components, respectively. The two lower frames present the corresponding dynamic spectra. At the time of the signal burst in By a w-shaped feature appears in the spectrum.

These W-shaped spectral features can be found rather frequently. They show a number of commonalities, but also some differences in details. In order to become more familiar with this spectral feature we introduce here the special characteristics. Figure 11 presents in the upper frames two classical cases. The oscillations start at the Nyquist frequency, decrease to zero, recover somewhat, before they go down to zero again; finally they rise and disappear beyond the Nyquist frequency. It is obvious from our standard spectrograms that the time resolution with a window length of 20 s is too coarse for resolving the temporal variations of the frequency changes properly. For that reason we

repeated for a number of events the spectral analysis with a window length of 128 data points (~2 s). Thanks to the sufficient signal-to-noise ratio our features are still well identifiable in this reduced spectral resolution. The examples in Figure 11 are from higher resolution spectra. They unveil a number of further details. In several cases we find a rising signal traces before the main signal appears at the Nyquist frequency. We interpret this as the presence of a higher frequency signal that is folded into the measurement range by the Nyquist phenomena. After the recovery from zero Hertz the frequency shows some variations. Interestingly, we can even identify signal bands of second and third harmonics of the fundamental frequency. At the end of the event the signal always disappears upward beyond the Nyquist frequency. Figure 12 presents a single spectrum through the middle part of the W-shaped feature, at a time when the frequency is quite stable over the analysis interval. One can clearly see that the oscillations have amplitudes of about 20 pT, well above the noise level. The obtained bandwidth of 1 Hz is quite narrow. These spectral characteristics are rather typical for all the events.

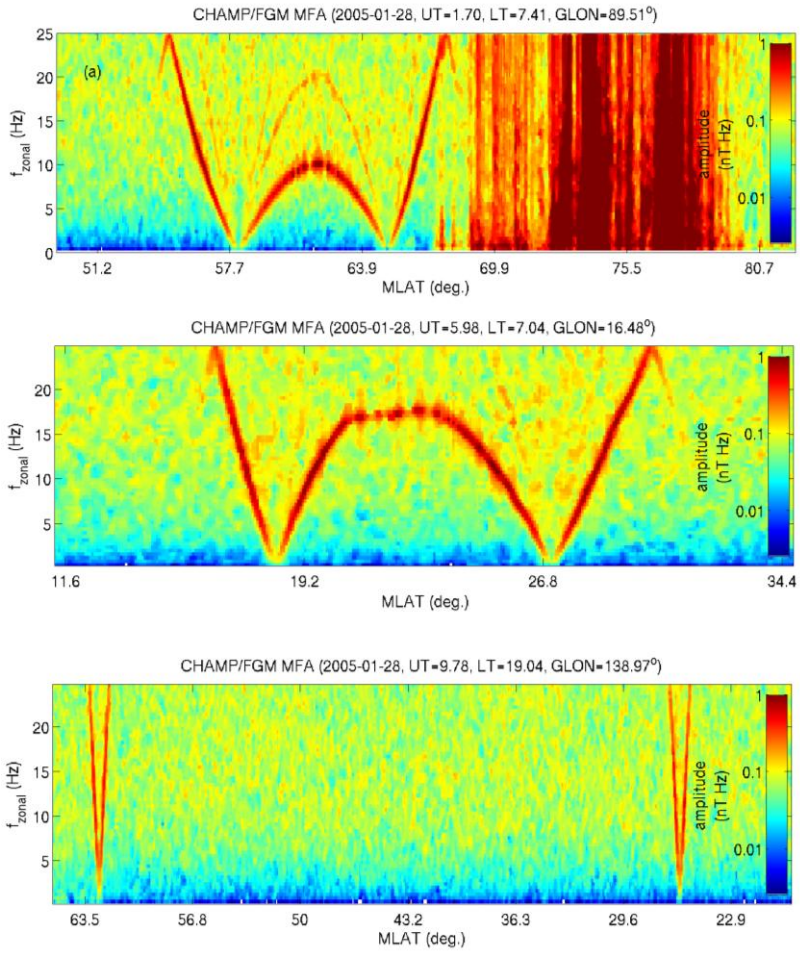

Figure 11. Examples of V- and W-shaped spectral features recorded by the By component. The spectral amplitudes have been multiplied by their frequency in order to pre-whiten the signal strength.

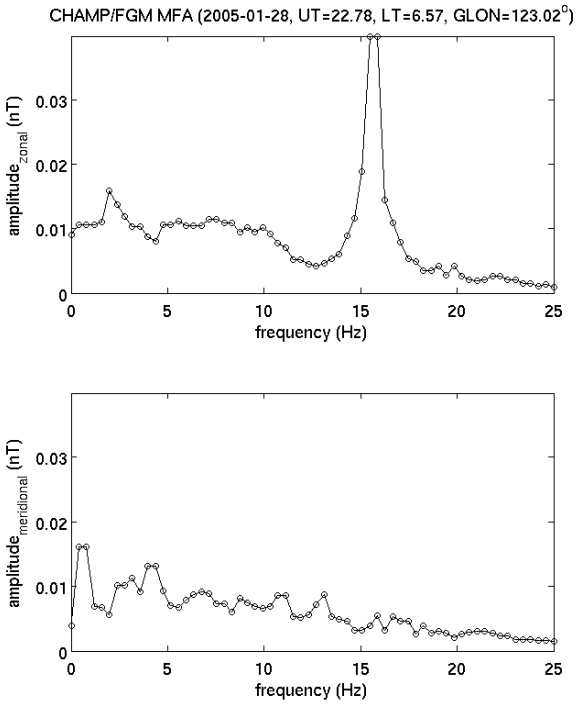

Figure 12. (top panel) Single spectrum from the central part of a W-shaped feature in the zonal component. The signal level is well above the noise. The bandwidth ranges around 1 Hz. (lower panel) Simultaneous spectrum of the meridional, B_x, component for comparison.

There is another kind of event. The spectral shape of that resembles more a "V". One example of that kind is shown in Figure 11, bottom frame. In those cases the frequency comes down from the ceiling, hits zero, and goes up again beyond the Nyquist frequency. These "V-events" can be found much more frequently than the W-shaped events. We think both kinds of features are related to the same effect thus we have studied them in one go.

We have surveyed the whole CHAMP data set and tried to identify all the V- and W-shaped events at middle and low latitudes. As can be seen in Figure 13, the events are not distributed evenly over the globe but form distinct patterns. There is a brought stripe running from north to south through the Americas. Another goes from Australia up to the Aleut Islands or to Europe. All these regions of dense red dots map out regions of small magnetic declination, as can be deduced from a comparison

with the geomagnetic declination map shown in Figure 13. This good correlation between the two very different quantities suggest that the V- and W-shaped signals in the B_y component are artificial.

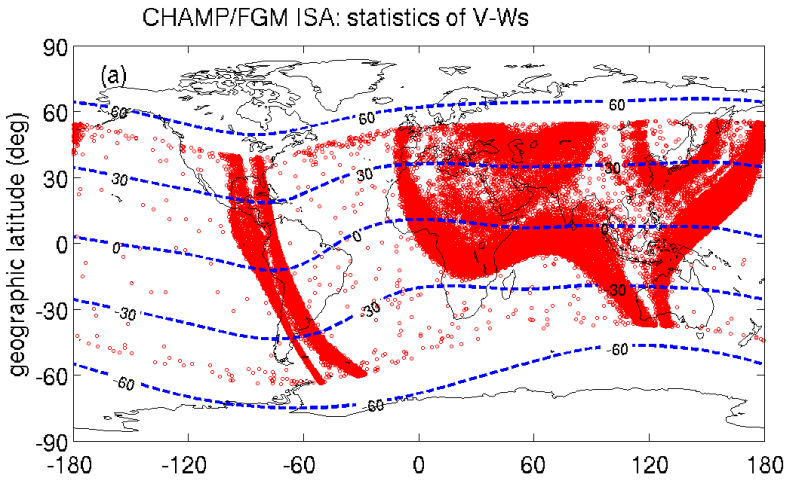

Figure 13. Global distribution of V- and W-shaped events. High latitudes are excluded be cause of too much false detection.

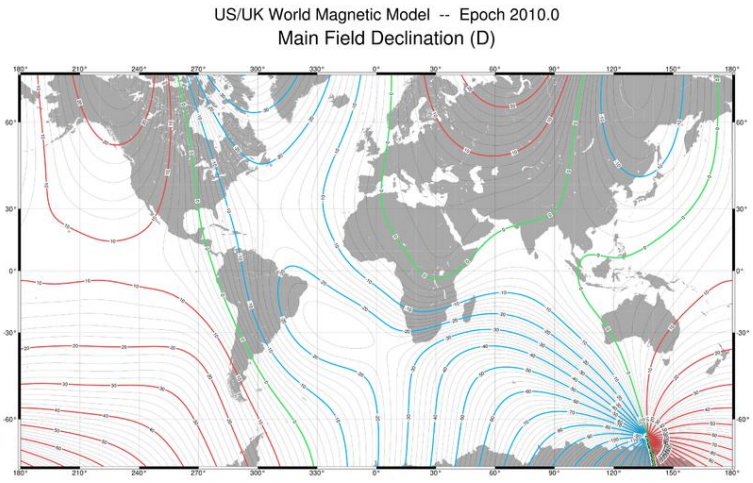

Figure 14. Global map of magnetic declination.

Concerning the root cause of the peculiar signal, we strongly suggest that it reflects an oscillation of the y component ADC at the crossover from negative to positive readings. It can be stated that the MFA y component is at middle and low latitudes rather well aligned with FGM y-axis. Therefore we

293 can affiliate our B_y observation with FGM y features. Since CHAMP flies almost over the poles, the
294 zero-declination lines are closely related to the change in B_y sign change. The declination map, Figure
295 14, confirms this inference. Furthermore, we observe a bifurcation of the event lines in Figure 13,
296 which is best visible over the Americas. The cause of that is the slight difference (2.3°) of the CHAMP
297 attitude from true north. On upleg orbital arcs events are found in regions of small eastward
298 declination and on downward arcs they appear at westward declination (figures not shown). Therefore,
299 the lines of true zero-declination are left more or less blank. The remaining question is, why do we
300 observe either V- or W-shaped spectral features? As the satellite approaches the zero-declination
301 region the Sigma-Delta ADC starts oscillating at a fairly high frequency. This decreases and stops
302 right at the y-axis sign change. At withdrawal from the zero line the frequency increases again. The V-
303 shaped features appear where we have a quick sign change, in regions where the zero-declination line
304 runs primarily in east-west direction, e.g. India or Indonesia (see Fig. 13). W-shaped features reflect
305 multiple sign changes of the y-axis. These are found in regions where the zero-declination line is
306 oriented north-south, e.g. Kamchatka, Siberia, Europe. Small satellite attitude variations of order 2°
307 are probably responsible here for the multiple zero crossings. We have also looked into the other two
308 FGM components. They also show indications of oscillation at sign changes but with much lower and
309 insignificant amplitudes.
310
311 **4. Conclusions and Summary**
312 Our survey of the high-resolution CHAMP magnetic field data at 50 Hz over ten years of mission live
313 revealed the quality of the data. The ADC provides a resolution 10 pT (least significant bit) that allows
314 for an unprecedented magnetic field data set in the ELF frequency range up to 25 Hz. There are three
315 kinds of distinct disturbance features. The largest artificial signal appears during a sign change of the
316 FGM y-axis. We observe a sweep through the whole frequency range, first downward then upward as
317 the satellite crosses the zero-declination line. The amplitude at which the frequency the ADC is

318 oscillating amounts to 40 pT. The other two FGM components also show oscillations at zero crossing
319 but at insignificantly low amplitudes.
320 The second largest contribution to the artificial signal comes from the star sensor units on the optical
321 bench at 2.1 Hz and higher harmonics. The ASC emits narrow pulses at 0.5 s separation and about 0.1
322 nT amplitude during times of partial blinding by the sun and/or the moon. Disturbance amplitudes
323 from the camera head on the A-side of the satellite are larger by a factor of about 2 than those from the
324 B-side. The FGM x-axis is most affected by this disturbance. Here the amplitudes spectral lines reach
325 25 pT. The y-axis shows only half the amplitude and the z-axis is practically not affected.
326 Finally, the FGM x-axis exhibits a continuous ringing at exactly 8 Hz. The amplitude of the signal is
327 temperature dependent. At a typically low operational temperature of 15°C we observe amplitudes of
328 about 12 pT at 8 Hz. This value decreases as the temperature rises. At values above 20°C the ringing
329 practically disappears. We cannot give a convincing explanation for the cause of the FGM x-axis
330 ringing. This 8 Hz signal is close to the Schumann resonance. It thus has to be taken carefully into
331 account when searching for that resonance in the topside ionosphere.

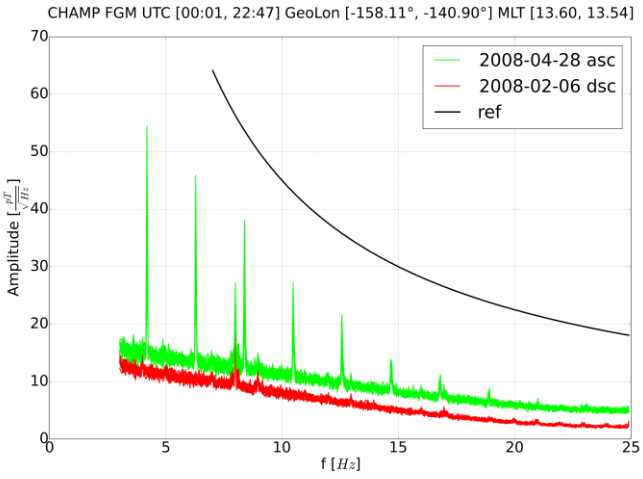

Figure 15. Summary of CHAMP FGM noise features. (green) a typical dayside pass; (red) a nightside pass on a Wednesday; (black) noise level as specified for CHAMP. The red and green curves are average spectra over the -50° to 50° magnetic latitude range. On Wednesdays the overall noise level is reduced, see text.

There is an operational feature of the FGM, worth to be mentioned here. During normal operation the FGM data are compressed before transmission. This reduces the data volume by a factor of 3. But on every Wednesday the full 24-bit FGM readings are transmitted. From figure 15 it is evident that without compression (lowest curve) the resolution of the FGM readings is generally improved by about 3 $pT/Hz^{1/2}$ over the presented frequency range. This shows the advantage of considering Wednesdays for high-resolution studies.

Figure 15 provides a kind of summary of the different noise features. The black line marks the CHAMP Mission Requirement for the noise level of the FGM data. Overall the actual noise floor is well below the requirement. The signal curves are a superposition of the 15 passes per day averaged over the -50° to 50° magnetic latitude range. The green curve is from a day with strong disturbances (MJD 3215). All the spectral features are well below the required level. In general there is a margin of a factor of 4 between the observed CHAMP noise floor and the requirement. On Wednesdays this is even more.

In summary, we can state an excellent performance of the CHAMP FGM in the frequency range 1-25 Hz. Only some distinct frequency lines are affected by artificial signal (2.1 Hz and higher harmonics, 8 Hz). The general noise floor is well below specification and is even lower on Wednesdays. All this qualifies the CHAMP FGM data for systematic studies in the ELF range over the mission period 2000-2010. The available frequency range up to 25 Hz has in the past only sparsely been investigated.

Acknowledgments

The authors acknowledge the CHAMP data processing team at GFZ, German Research Centre for Geosciences, Section 2.3 'Earth's Magnetic Field' for continuous support. The CHAMP mission was sponsored by the Space Agency of the German Aerospace Center (DLR) through funds of the Federal Ministry of Economics and Technology. The work of FY was supported by the National Natural

Science Foundation of China (Grant No. 41104119 and 41474157). Large part of the work presented here was performed during a research visit of FY at GFZ.

FY furthermore thanks the referees for their comments and suggestions to improve the paper.

References

Lühr H, Yin F and R. Bock 2013 Magnetic properties of CHAMP and their effects on in-flight calibration *Journal of Sensors and Sensor Systems* 2 9-17

Lühr H, Xiong C, Park J and Rauberg J 2014a Systematic study of intermediate-scale structures of equatorial plasma irregularities in the ionosphere based on CHAMP observations, *Front. Physics 2:15*, doi: 10.3389/fphy.2014.00015.

Lühr H, Park J, Xiong C and Rauberg J 2014b Alfvén wave characteristics of equatorial plasma irregularities in the ionosphere derived from CHAMP observations, *Front. Phys. 2:47*, doi:10.3389/fphy.2014.00047.

Ni B.B, Zhao Z.Y 2005 Spatial observations of Schumann resonance at the ionospheric altitude *Chinese Journal of Geophysics* 48 818-826

Park, J. and H. Lühr 2012, Effects of sudden stratospheric warming (SSW) on the lunitidal modulation of the F-region dynamo, *J. Geophys. Res., 117,* A09320, doi:10.29/2012JA018035.

Park J, Lühr H, Rauberg J 2013 Global characteristics of Pc1 magnetic pulsations during solar cycle 23 deduced from CHAMP data *Annales Geophysicae* 31 9 1507-1520,

Reigber Ch, Lühr H and Schwintzer P 2002 CHAMP mission status *Adv. Space Res.* 30 2 129-134

Rother M, Schlegel K, Lühr H 2007 CHAMP observation of intense kilometre-scale field-aligned currents, evidence for an ionospheric Alfvén resonator *Annales Geophysicae* 25 7 1603-1615

Schumann W. O. 1952 On the free oscillations of a conducting sphere which is surrounded by an air layer and an ionosphere shell (in German) *Z. Naturforsch.* B 7A 149-154

Simoes F.A, Pfaff R.F, Freudenreich H.T 2011 Satellite observations of Schu-mann resonances in the Earth's ionosphere *Geophysical Research Letters* 38 22101

382 Surkov V.V, Nosikova N.S, Plyasov A.A, Pilipenko V.A, Ignatov V.N 2013 Penetration of Schumann
383 resonances into the upper ionosphere *Journal of Atmospheric and Solar-Terrestrial Physics* 97
384 65-74
385 Yin F, Lühr H, Rauberg J, Michaelis I, Cai H.T 2013 Characterization of CHAMP magnetic data
386 anomalies: magnetic contamination and measurement timing *Measurement Science and*
387 *Technology* 24 075005
388

Biography of the author

Dr. Fan Yin, born in 1976, graduated in electronics (bachelor) and in space-physics (Master) from Wuhan University, China. In 2010 he obtained his doctor's degree from University of Potsdam and Helmholtz-Centre Potsdam, GFZ-German Research Centre for Geosciences, Germany. Now he is a lecturer in Wuhan University. His current fields of interest include space observation, instrument calibration/data validation and dynamic processes in the ionosphere.

List of the figure captions

P4

Figure 1. Schematic illustration of the CHAMP satellite (top) and a schematic relationship between CHAMP attitude in orbit and sunlight (bottom).

P7

Figure 2. Noise spectrum of one day: superposed PSD of B_z (in MFA) for MJD 3215. (upper left) ascending arcs at 01:34 OLT, (lower left) descending arcs at 13:34 OLT; (right frame) zoomed spectrum with sidebands of the 8 Hz signal.

P8

Figure 3. Dynamic noise spectrum of B_z (in MFA) for MJD 3208. (lower frame) latitudinal of CHAMP position (blue: ascending arcs; red: descending arcs). Local time of the ascending node is 02:13 OLT.

P9

Figure 4. Event distributions of 2.1 Hz harmonic signals. (top) event occurrence in time-latitude frame; (bottom) magnitude distribution in time-magnitude frame.

P12

Figure 5. Upper: Event distributions of 2.1 Hz harmonic signals with respect to moon elevation. (top) color coded event occurrence in time-latitude frame; (bottom) event distribution on the nightside.

P13

Figure 6. Event distributions of 2.1 Hz harmonics at expanded scale. (top panel) event occurrence in time-latitude frame over 60 days; (middle panel) PSD magnitude distribution; (bottom frame) details of event occurrences over 10 days. The red stripes mark events caused by moonlight.

P13

Figure 7. Day-to-days event distributions of the 2.1 Hz harmonics in a longitude-latitude frame spanning MJD3180-3189. Warm colors reflect high PSD magnitudes. Data from the nightside are excluded.

P15

Figure 8. Temperature dependence of 8 the Hz signal. (top) event occurrence in time-latitude frame; (middle panel) magnitude distribution in time-magnitude frame; (bottom frame) temperature variation of the magnetometer ADC.

P15

Figure 9. Global event occurrence distributions of the 8 Hz signal in the three MFA components: B_z top, B_x middle, B_y bottom, for the year 2008. The lines in the two upper frames represent magnetic inclination, in the bottom frame it is magnetic declination.

P17

Figure 10. Example of a W-shaped event. The two panels (a) and (b) show time series of the MFA B_y and B_x components, respectively. The two lower frames present the corresponding dynamic spectra. At the time of the signal burst in By a w-shaped feature appears in the spectrum.

P19

446 **Figure 11.** Examples of V- and W-shaped spectral features recorded by the By component. The
447 spectral amplitudes have been multiplied by their frequency in order to pre-whiten the signal strength.
448
449 P20
450 **Figure 12.** (top panel) Single spectrum from the central part of a W-shaped feature in the zonal
451 component. The signal level is well above the noise. The bandwidth ranges around 1 Hz. (lower panel)
452 Simultaneous spectrum of the meridional, B_x, component for comparison.
453
454 P21
455 **Figure 13.** Global distribution of V- and W-shaped events. High latitudes are excluded be cause of too
456 much false detection.
457
458 P21
459 **Figure 14.** Global map of magnetic declination.
460
461 P23
462 **Figure 15.** Summary of CHAMP FGM noise features. (green) a typical dayside pass; (red) a nightside
463 pass on a Wednesday; (black) noise level as specified for CHAMP. The red and green curves are
464 average spectra over the -50° to 50° magnetic latitude range. On Wednesdays the overall noise level is
465 reduced, see text.
466

Highlights

- We have investigate all signals from 1Hz to 25Hz based on the years of the CHAMP 50 Hz vector magnetic data. The available frequency range up to 25 Hz has in the past only sparsely been investigated.
- Three types of disturbances are found regularly in the data. One is at ~2.1Hz and harmonic signals, an other is an 8Hz single frequency signal. The third artificial signal affects the FGM y-axis which sweeps from the Nyquist frequency down to zero and up again occurs when the readings of the FGM y-axis go through zero.
- The features of these signals are characterized and analyzed, which helps us to trace the signals to the source of disturbance e.g. nearby instruments or magnetometer.
- Our results qualify the CHAMP FGM data for systematic studies in the ELF range over the mission period 2000-2010.